Engineering Structures 122 (2016) 144–155

Contents lists available at ScienceDirect

Engineering Structures

journal homepage: www.elsevier.com/locate/engstruct

Behavior of prestressed concrete-filled steel tube (CFST) beam

Yulin Zhan [a,b], Renda Zhao [a], Zhongguo John Ma [c,d,*], Tengfei Xu [a], Ruinian Song [a]

[a] Department of Bridge Engineering, School of Civil Engineering, Southwest Jiaotong University, Sichuan 610031, China
[b] Key Laboratory of High-speed Railway Engineering, Ministry of Education, Sichuan 610031, China
[c] Department of Civil and Environmental Engineering, University of Tennessee, Knoxville, John D.Tickle, TN 37996-2313, USA
[d] School of Civil Engineering, Southwest Jiaotong University, Sichuan 610031, China

ARTICLE INFO

Article history:
Received 9 May 2015
Revised 7 February 2016
Accepted 25 April 2016
Available online 26 May 2016

Keywords:
Concrete-filled steel tube
Prestressed concrete
Strength
Ductility
Confinement

ABSTRACT

Concrete-filled steel tube (CFST) member is widely used for building, bridge and foundation structures because of its excellent performance. When a CFST member is subjected to axial loads, the filling concrete is confined by the steel tube, resulting in a tri-axial state of compression that improves its strength, stiffness and ductility. However, the cracking of concrete in tension zone would decrease this enhancement when the CFST member is subjected to flexure, especially when it is used as a major flexural member with large-scale section in bridges. To overcome this weakness, the prestressed CFST concept is investigated in this paper. Eight prestressed CFST beams with large-scale section (300 × 450 mm) were tested under bending. Two concrete strengths (C50 and C60) and two different degrees of prestressing (0.26 and 0.40) were studied in the experimental program. The full vibration and grouting method was introduced to gain a good performance of specimens. The perfobond rib shear connector was adopted to achieve the composite action. The flexural behaviors were verified by comparing with predictions from a proposed model considering the confinement effects. A simplified method is proposed to determine the ultimate moment capacity based on the plastic stress block hypothesis. Both experimental and analytical results show that the prestressed strands could significantly enhance the confinement effect of the core concrete under bending, which, in turn, improves the prestressed CFST beam performance in strength, stiffness and ductility.

Published by Elsevier Ltd.

1. Introduction

Concrete-filled steel tube (CFST) members are composite structures which evolved on the basis of the hollow steel tube (HST). For the hollow steel tube, local buckling of the flange may occur when the width-to-thickness ratio (B/t) is larger than a certain value [27,54,23]. Thus, the plastic bending moment of an HST beam may not be achieved or maintained. Filling concrete is an efficient way to prevent local buckling and to enhance performance of HST beams. Although the filling concrete would increase the dead weight to a certain level, it is still considered an efficient way to enhance strength, stiffness and ductility of HST members. Zhao and Grzebieta [55] proved that the increase in rotation angles of CFST members at ultimate moment can be three times larger than that of HST beams. CFST members can provide an excellent seismic resistance in two orthogonal directions as well as show good damping characteristics. They also show an excellent hysteresis behavior under cyclic loading when compared with HST tubes [21]. CFST members have been used in tall structures and in retrofitting damage bridge piers in USA and Japan [15]. The use of CFST members in moment resisting frames eliminates the need for additional stiffness elements in panel zones and zones of high strain demand [14]. Bridges with CFST members are expected to reduce noise and vibration levels when compared to ones with pure steel members [35]. Moreover, CFST members have been proven to be cost effective in building structures [50]. The example of Aurora pedestrian arch bridge does demonstrate that the CFST is an appealing modular system and is easy to fabricate and erect [44].

Many research efforts on the compressive behavior of CFST have been carried out in the past decades, however, the flexural performance of CFST is still very limited. Earlier studies on CFST beams were published by Furlong [16] and Bridge [5]. Furlong [16] found that the flexural capacity of CFSTs was increased by 49% compared to the bare steel tube beam. Bridge [5] also observed that the core concrete can provide approximately 7.5% more bending capacity than the hollow steel section. After these earlier studies, investigations were mainly focused on the depth-to-width ratio [33], shear span-to-depth ratio [37], and width-to-thickness ratio [46]. Uy [47] demonstrated that the CFST member had a significant yielding

* Corresponding author at: Department of Civil and Environmental Engineering, University of Tennessee, Knoxville, John D.Tickle, TN 37996-2313, USA.

http://dx.doi.org/10.1016/j.engstruct.2016.04.050
0141-0296/Published by Elsevier Ltd.

Nomenclature

B, H	the outer width and height of the section, respectively
λ	the degree of prestress
M_0	the decompression moment that produces zero concrete stress at the extreme fiber of the section nearest to the centroid of prestressing force when added to the action of effective prestress
M_u	the ultimate moment
σ_h	the effective compressive prestressing at tensile edge
W_0	the flexural modulus
E_s	the Young's modulus of steel
f_y	the yield strength of steel
f_u	the ultimate tensile strength of steel
e_u	the percentage elongation at fracture of steel
f'_c	the compression strength of concrete
f_t	the tensile strength of concrete
E_c	the Young's modulus of concrete
σ_{ps}, ε_{ps}	stress and strain of prestressed strand, respectively
E_p	the Young's modulus of prestressed strand
E'	the slop at the original point of Ramberg–Osgood curve
m	the coefficient for Ramberg–Osgood curve shape
μ_ϕ	the curvature ductility
ϕ_u	the curvature at ultimate when the steel fiber reaches a specified limiting value
ϕ_y	the curvature when the tension fiber first reaches the yield strength.
A_p	the area of prestressed strand
N_{s1}	the force of upper compressive flange zone for steel tube
N_{s2}	the force of compressive web zone for steel tube
N_{s3}	the force of tension web zone for steel tube
N_{s4}	the force of underside tension flange zone for steel tube
C	*the force of compressive flange zone for filled concrete*
X	the height of compression concrete
t	the thickness of steel tube
b, h	the inner width and height of the steel tube
f_p	the ultimate strength of prestressed strand
a_p	the distance from the center of prestressed strands to the outside edge of steel tube
M_{lb}	the buckling moment

plateau because of the high strength steel. Similarly, a favorable post-yield behavior of CFST member was reported by Gho and Liu [18]. The distinguishing feature of ductile collapse and smooth loading process was further studied based on the unified theory by Han [22] and Han et al. [24]. Finite element method [32], simplified analytical method [26] and cross-sectional fiber analysis [41] were proposed to predict the stiffness and bending strength. Eichalakani and Zhao [12,13] found that the static strength of CFST member was significantly influenced by cyclic loading.

Although previous studies have proved that the CFSTs had outstanding strength capacity, ductility, and seismic performance, Nakamura et al. [35] noted that the composite bending stiffness of CFST was similar to the theoretical stiffness of the bare steel tube due to the concrete cracking. Wheeler and Bridge [51] also found that the concrete cracking in tension zone in the early loading stage would significantly decrease the ultimate capacity to a value extremely close to the stiffness of bare steel section. The cracking moment was around 5% of ultimate moment. Chitawadagi and Narasimhan [8] reported that the increase of concrete strength relative to a given thickness tube did not increase the moment capacity to a great extent. It is hypothesized that cracking may cause the confinement degradation, which, in turn, results in the reduction of strength, stiffness and ductility in CFST beams. Therefore, a modified CFST named as prestressed CFST, is proposed here in order to reduce these deficiencies. The main idea is that the triaxial state of core concrete will be further strengthened by the combined effect of steel tube and prestressed strands. Chen et al. [7] and Xu et al. [53] have discussed this proposed concept in theory. Tuan [44,45] also studied the prestressed CFST as an axial tension member and successfully applied it as the bottom chords in a pedestrian arch bridge in Aurora, NE (Fig. 1).

This paper focuses on the flexural performance of prestressed CFST beams under bending. All specimens have the same compact section (300 × 450 mm). Two concrete strength (C50 and C60) and two different degrees of prestressing (0.26 and 0.40) were investigated in the experimental program. The full vibration and grouting method was introduced to gain a good performance of the specimens. Additionally, both three-point and four-point loading setups were applied for the loading program in order to study the influence by loading pattern. A theoretical model was introduced to study the moment–curvature relationship. A simplified method was proposed to predict the ultimate moment capacity based on the plastic stress block hypothesis. Experimental and theoretical results demonstrate that the prestressed strand could increase the confinement effect of the core concrete under flexure, and the prestressed CFST beam performs well in terms of its strength, stiffness and ductility.

2. Experimental program

2.1. Parameters of specimens

A total of eight specimens were designed and prepared to investigate the flexural behavior. The specimens were fabricated from cold-weld steel hollow sections, and two different strength concretes were filled. The dimensions of the specimens are showed in Fig. 2. All specimens have the same outer width of 300 mm and the same height of 450 mm. CFST members are usually classified as a compact section, non-compact section or slender element section according to the local buckling potentials of the steel tube. And the width-to-thickness ratio (B/t) is used to measure the local buckling potential for rectangular CFST members. Currently, there exist differences on B/t limit value specified in different codes [1,4,10]. Most codes define the B/t limit with the elastic modulus and the yield strength of steel. For a rectangular hollow steel tube, flange plane is slenderer than web plane, thus the section type mainly depends on the width-to-thickness (B/t) of flange. Although there are a few differences in the definition of B in existing codes, a unified expression of B is defined as the outer width of the section in this paper. The comparison among different codes is illustrated in Table 1. Table 1 shows that all specimens with nominal B/t ratios of 50 and 37.5 satisfy the limits. In order to investigate the prestressing effect, the degree of prestress, λ, is defined as follows [34]:

$$\lambda = \frac{M_0}{M_u} \tag{1}$$

$$M_0 = \sigma_h W_0 \tag{2}$$

where λ = the degree of prestress; M_0 = the decompression moment that produces zero concrete stress at the extreme fiber of the section nearest to the centroid of prestressing force when added to

(a) Schematic of Aurora arch bridge (b) prestressed CFST used as bottom chords

Fig. 1. Pedestrain arch bridge in Aurora, NE (USA).

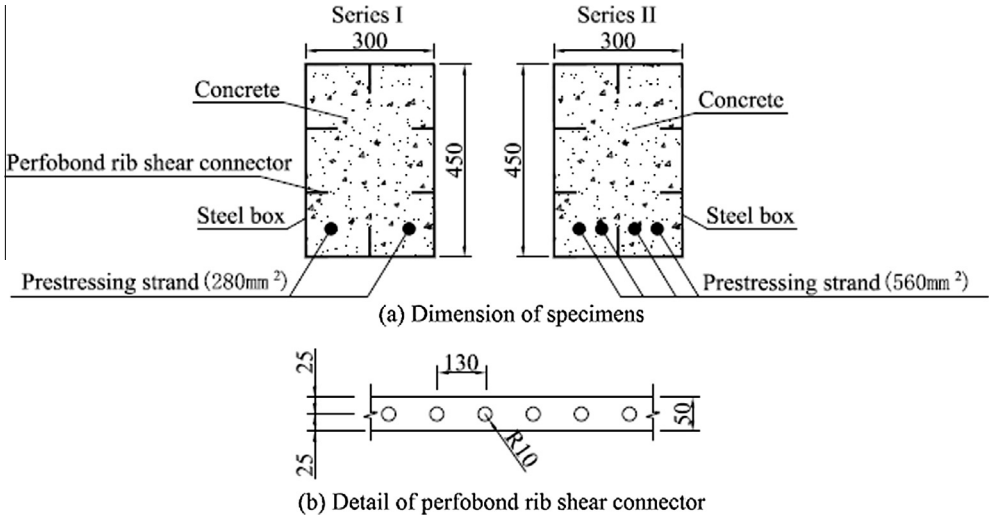

Fig. 2. Test specimens (unit: mm).

Table 1
Comparison of the width-to-thickness ratio (B/t).

Type	t (mm)	Nominal B/t ratio	Measured B/t ratio	Code		
				AISC	EC4	AIJ
N1	6	50.0	50.3	51	53	73
N2	8	37.5	38.4	51	53	73

the action of effective prestress; M_u = the ultimate moment; σ_h = the effective compressive prestressing at tensile edge; W_0 = the flexural modulus.

The parameters for all specimens are listed in Table 2.

2.2. Concrete

According to the AISC code (2010), concrete shall have a compressive strength, f'_c, of not less than 21 MPa (3.0 ksi) nor more than the 70 MPa (10.0 ksi) for normal weight concrete. Two concrete mixes with design strength of 50 MPa (C50) and 60 MPa (C60) were used. The mixes are shown in Table 3. The maximum diameter of coarse aggregate is less than 25 mm, and the medium diameter sand was used as the fine gravel aggregate. Coarse aggregates were washed and dried before mixing. Additives to increase the viscosity or fillers were also used. The concrete material properties were determined by conducting uniaxial compression tests according to ASTM [3] standards on 150-mm concrete cylinders. The properties of concrete are shown in Table 4.

Table 2
Parameters of specimens.

Specimens	Type	Prestressing strand	λ	Steel proportion (%)	Concrete	Loading mode
S-1	N1	Series I	0.26	6.67	C50	Four-point
S-2	N2	Series I	0.26	8.89	C50	Three-point
S-3	N1	Series II	0.40	6.67	C50	Four-point
S-4	N2	Series II	0.40	8.89	C50	Three-point
S-5	N1	Series I	0.26	6.67	C60	Four-point
S-6	N2	Series I	0.26	8.89	C60	Three-point
S-7	N1	Series II	0.40	6.67	C60	Four-point
S-8	N2	Series II	0.40	8.89	C60	Three-point

Table 3
Concrete mixes.

Materials	C50 (kg/m^3)	C60 (kg/m^3)
Cement	452	543
Water	212	190
Coarse aggregate	1229	1167
Sand	529	500
Water-reducing admixture	4.2	5.3

Table 4
Properties of concrete.

Type	f_t (MPa)	f'_c (MPa)	E_c (MPa)
C50	4.25	53.90	3.27×10^4
C60	4.24	57.90	3.47×10^4

Table 5
Properties of Steel.

Thickness (mm)	f_y (MPa)	f_u (MPa)	YR	e_u (%)	E_s (MPa)
4	285.9	404.7	0.71	30.18	2.05×10^5
6	277.6	396.6	0.70	31.26	
8	303.4	448.4	0.68	32.06	
Average	289.0	416.6	0.70	31.17	2.05×10^5

2.3. Steel and prestressed strand

Two thickness steel plates (6 mm and 8 mm) were used to fabricate the tube. And 4 mm-thick steel plate was selected for the perfobond rib shear connector (Fig. 2). A perfobond rib shear connector consists of a steel plate with a number of holes uniformly spaced. When the holes in the perfobond rib are filled with concrete, concrete dowels are formed. The dowels provide horizontal shear resistance between steel and concrete. Additionally, the perfobond rib shear connector is also used as the stiffness rib which can prevent warping of the steel plate during welding. According to AISC code (2010), the specified minimum yield stress of structural steel used in the rectangular concrete filled steel tube shall not exceed 525 MPa (75 ksi), thus Grade A was adopted for all specimens. The steel material properties of the CFST specimens were determined by conducting uniaxial tension tests according to ASTM [2] standards on coupons that were cut and machined from the side of the steel tube. Table 5 shows the values of f_y, f_u, YR, e_u, and E_s which are the measured average yield strength, ultimate strength, yield-to-ultimate strength ratio (f_y/f_u), percentage elongation at fracture and Young's modulus, respectively. The prestressed strand, Grade 270 with 0.6 in. diameter, was used for all specimens.

2.4. Fabrication of test specimens

Different pouring patterns would result in different concrete bonding strength, and thus four different pouring patterns had been investigated by Virdi and Dowling [49]. The first two patterns (Pattern I and II) adopted full and light vibration after pouring, respectively. The third pattern (Pattern III) divided the pouring into three steps, and 40 times vibration was applied after each pouring. The last pattern (Pattern IV) was similar to the third one except that the vibration time was changed to 20 times. The results show that the pouring pattern greatly influenced the bonding strength. In order to get an effective bonding strength, Pattern I was used in this study. Previous research also showed that an incomplete grouting can result in the loss of prestressing force over a significant distance, which, in turn, can cause an appreciable increase in deflection [6]. Thus, a high quality grouting was applied to all. As shown in Fig. 3, specimen construction steps are as follows: (1) Install the perfobond rib shear connector, and then weld four steel plates to form a rectangular tube; (2) Rotate the tube to the vertical direction in order to fill the concrete; (3) Place steel pipes at the designed locations to create ducts for pulling the prestressed strand through; (4) Fill the tube with concrete and vibrate the

Fig. 3. Specimens construction steps.

concrete from the top; (5) Cure the concrete to reach 70% of its design strength, and then prestress the strand; (6) Grout the ducts.

The effective stress of prestressed strand was measured by the loading transducer at each end of the strand. Table 6 presents the measured effective stress of prestressed strand compared with the expected values.

2.5. Test setup and procedure

A schematic view of the test set-up and a picture of a specimen in the testing rig are shown in Fig. 4. All specimens were tested to failure under bending with a span of 5000 mm. Three-point and four-point loading patterns were applied to the specimens. The applied loads were measured through the actuator transducer. The vertical deformations were measured using three Linear Potentionmeters positioned along the length of the span. The support settlements were also measured. Strain gauges were positioned at the mid-span section of each specimen. The specimens were tested under 1000 kN MTS servohydraulic actuator. Initially, two cycles of preloading up to 100 kN (about 10% of the expected failure load) with a rate of 5 kN/s were conducted to check the experimental device and instruments. In the subsequent loading stage, instruments were initialized and the loading was applied in small increments of 20 kN. When the loading exceeded the cracking moment, the loading increment was changed from 20 kN to 50 kN. After the steel yielded, the loading was changed to displacement control, which would record the softening behavior of the specimen.

Table 6
Effective prestressing stress values.

Specimens	Measured value (MPa)	Calculated value (MPa)	Ratio	Ratio to ultimate strength
S-1	942.86	948.57	0.99	0.51
S-2	1125.71	1115.71	1.01	0.61
S-3	915.71	930.00	0.98	0.49
S-4	997.86	1041.43	0.96	0.54
S-5	915.00	892.86	1.02	0.49
S-6	1059.29	1060.00	1.00	0.57
S-7	867.86	874.29	0.99	0.47
S-8	1007.86	985.71	1.02	0.54

A typical criterion of the loading termination was proposed as the moment dropped to a certain level of the maximum moment [19]. The beginning of concrete crushing in compression accompanied by steel yielding in tension or local buckling in compression was another quintessential method to determine the failure [17,40]. Any tensile fiber of steel reached a specified rupture strain was the third termination [20]. The dropped moment criterion usually applied to CFST with a high B/t ratio subjected to high axial loads [9]. The beginning of the concrete crushing or steel stress reached a tensile strength does not necessarily mean the loss of capacity immediately, especially when the concrete was in the confined state [9]. Furthermore, the moment still tends to stabilize even when the maximum strain of steel reached 0.01[22]. Thus, for practical consideration, the moment corresponding to the maximum steel strain of 0.1 was defined as the ultimate moment (M_u).

3. Results and discussions

3.1. Moment–curvature characteristics

Though the specimens were designed by different nominal B/t ratios, material strengths, degrees of prestressing and loading patterns, the moment–curvature ($M-\phi$) shapes at the mid-span section follow the similar law. Significant events during the test, indicated on the $M-\phi$ response curve shown in Fig. 5, are as follows: (A) concrete starts to crack; (B) steel flange in compression starts to yield; (C) extreme concrete fiber reaches the compressive strain ε_{cu} (ε_{cu} = 0.0035); (D) steel flange in tension starts to yield; (E) prestressed strand starts to yield; (F) local buckling of compression flange initiates; (G) specimen reaches M_u. Events A, B, C and D were established using the longitudinal strains that were measured at the upper and bottom edge of the mid-span section. Events E and F were experimental observations as well as the determination from moment–curvature curve. Event G indicated that the longitudinal strain of steel exceeded the maximum steel strain.

3.2. Strength

Although Wheeler and Bridge [51] reported that the cracking would occur when the load reached to about 5% of the ultimate

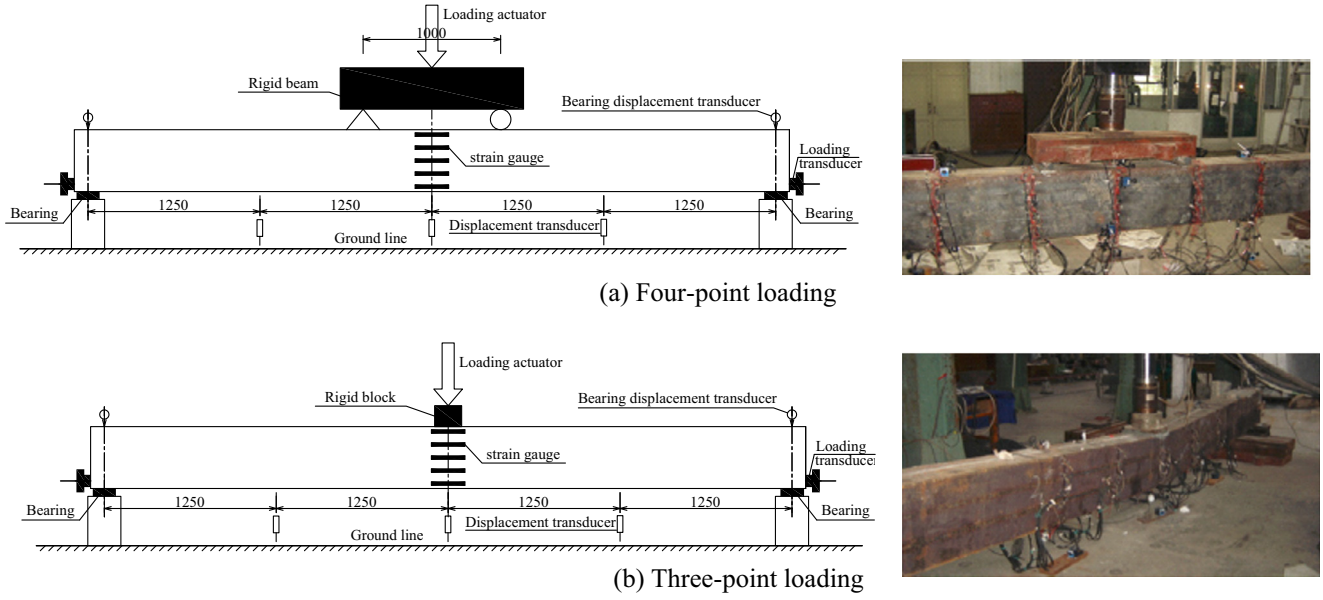

Fig. 4. Schematic test set-up.

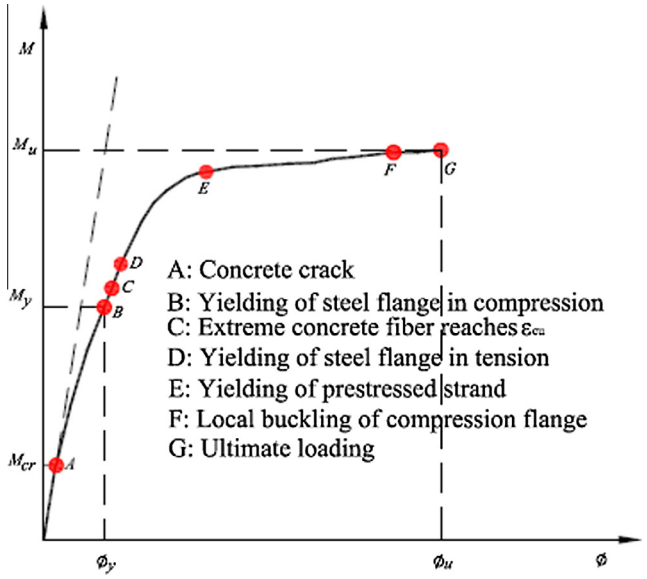

Fig. 5. $M-\phi$ curve of mid-span.

Table 7
Results of characteristic moments.

Specimens	M_{cr} (kN m)	M_y (kN m)	M_u (kN m)	M_{cr}/M_u	M_y/M_u
S-1	135	400.00	611.40	0.22	0.65
S-2	130	593.75	878.63	0.15	0.68
S-3	210	489.20	770.40	0.27	0.63
S-4	190	684.38	1037.88	0.18	0.66
S-5	130	460.30	729.10	0.18	0.63
S-6	130	627.63	893.63	0.15	0.70
S-7	190	493.50	790.10	0.24	0.62
S-8	170	688.75	1072.50	0.16	0.64
Average				0.19	0.65

load for normal CFTS beams, the cracking moment of the prestressed CFST beam is 19% of the ultimate moment (M_u) as shown in Table 7. At about 0.65 M_u, yielding of the steel tube occurred with the increasing flexural deformation. At around 0.90 M_u, the prestressed strand reached to its yield strength as demonstrated by a considerable slope reduction in the moment–curvature curves. The specimens achieved their moment capacity and failed to load further due to the strain exceeding the limit.

Fig. 6 shows the influence of different testing parameters on the ultimate moment (M_u). Fig. 6(a) indicates that the increase of the width-to-thickness ratio reduces the ultimate moment by an average of 25%. Fig. 6(b) and (c) demonstrate that both the degree of prestress and the concrete strength can have an impact on the ultimate moment.

Table 8
Results of curvature ductility and deformation.

Specimens	ϕ_y (1/m)	ϕ_u (1/m)	μ_ϕ	Δ_u (mm)	Δ_u/L
S-1	0.0067	0.0662	9.91	167.58	30
S-2	0.0063	0.0619	9.79	156.90	32
S-3	0.0062	0.0715	11.56	181.13	28
S-4	0.0063	0.0779	12.36	197.41	25
S-5	0.0064	0.0716	11.17	181.39	28
S-6	0.0069	0.0544	7.91	137.77	36
S-7	0.0063	0.0594	9.36	150.38	33
S-8	0.0064	0.0741	11.55	187.74	27
Average	0.0064	0.0671	10.45	170.03	30

3.3. Ductility

Ductility can be defined as the ability of the specimen to undergo deformation without a substantial reduction in the flexural capacity [36]. The curvature ductility, μ_ϕ, is defined as following:

$$\mu_\phi = \frac{\phi_u}{\phi_y} \tag{3}$$

where ϕ_u = the curvature at ultimate strength when the steel fiber reaches a specified limiting value; ϕ_y = the curvature when the tension fiber first reaches the yield strength.

The results of curvature ductility and maximum deflection are shown in Table 8. The average curvature ductility is 10.45 and the average deformation is 1/30 of the span length. The specimen had an excellent ductility under bending.

3.4. Stiffness

In order to calculate the effective modulus stiffness, Eq. (4) was typically used in AISC-LRFD (2010), EC4 [10], and AIJ [4].

$$EI = E_sI_s + \alpha E_cI_c \tag{4}$$

where EI = the effective modulus stiffness of composite section; E_s, E_c = the Young's Modulus of steel and concrete, respectively; I_s, I_c = the moment of inertia of steel and concrete, respectively; α = coefficient.

AISC-LRFD (2010), EC4 [10], and AIJ [4] define different values for coefficient α as 0.4, 0.6 and 0.2, respectively. According to Fig. 5, the initial flexural modulus stiffness, $(EI)_i$, was defined as the corresponding value when the moment reached to 20% of the ultimate moment. Table 9 illustrates the comparison between the testing results, $(EI)_i$, and predictions from different codes. The results show that the stiffness calculated from AISC-LRFD, EC4 and AIJ is about 56%, 75% and 50% of the initial stiffness from experiment, respectively. The prestressed strand has a significant

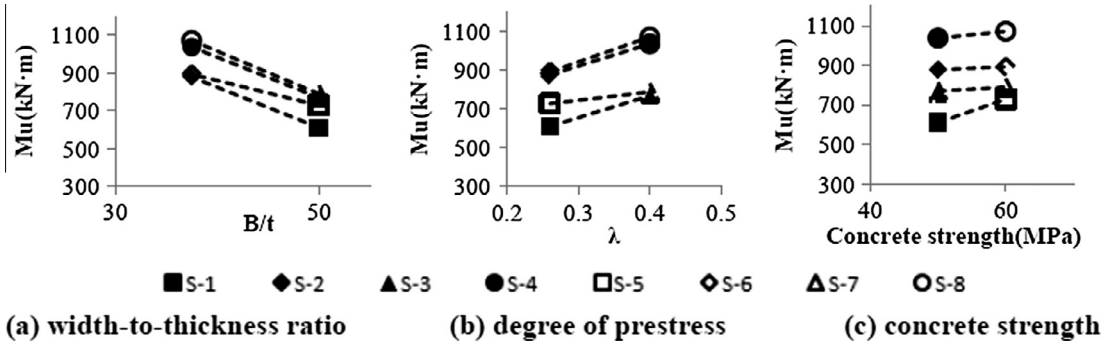

Fig. 6. Ultimate moment vs. testing parameters.

Table 9
Stiffness results.

Specimens	$(EI)_i$	AISC–LRFD		EC4		AIJ	
	(kN·m^2)	EI (kN·m^2)	$EI/(EI)_i$	EI (kN·m^2)	$EI/(EI)_i$	EI (kN·m^2)	$EI/(EI)_i$
S-1	95,655	52,450	0.55	71,020	0.74	45,578	0.48
S-2	76,282	60,883	0.8	79,451	1.04	54,920	0.72
S-3	96,918	52,792	0.54	72,055	0.74	45,922	0.47
S-4	178,416	61,225	0.34	80,486	0.45	55,265	0.31
S-5	95,681	52,204	0.55	70,610	0.74	45,578	0.48
S-6	94,568	60,637	0.64	79,041	0.84	54,920	0.58
S-7	92,934	52,546	0.57	71,645	0.77	45,922	0.49
S-8	118,181	60,979	0.52	80,076	0.68	55,265	0.47
Average			0.56		0.75		0.50

Table 10
Local buckling records.

Specimens	M_{lb} (kN·m)	M_u (kN·m)	M_{lb}/M_u	Position of local buckling
S-1	611.40	611.40	1.00	Near the loading point
S-2	–	878.63	–	No local buckling observed
S-3	741.30	770.40	0.96	Near the loading point in pure bending segment
	763.00	770.40	0.99	
	765.60	770.40	0.99	
S-4	993.84	1037.88	0.96	Near the loading point at mid-span section
S-5	688.40	729.10	0.94	In the pure bending segment
S-6	857.88	917.38	0.94	Near the loading point at mid-span section
S-7	788.60	790.10	1.00	In the pure bending segment
S-8	1052.52	1072.50	0.98	Near the loading point at mid-span section

Note: M_{lb} was defined as the moment when the local buckling occurred.

influence on the flexural stiffness due to the efficacious confinement effect.

3.5. Local buckling

Local buckling of the steel flange in compression was observed until the loading was increased to the ultimate moment level. Table 10 lists the local buckling moments and the locations where it occurs. Except the specimen S-2, all other specimens experienced local buckling. Most local buckling occurred near the loading point, as shown in Fig. 7, and the local buckling moment was close to the ultimate moment (Table 10). Four-point loading caused more serious local buckling than Three-point loading because of the high compressive stress in the segment of specimen between the two loading points. In addition, no local buckling in the webs was observed during the test. All specimens were opened to examine the filling concrete damage after test, and the separation between the steel plate and concrete around the local buckling point was found.

4. Analytical prediction modals

4.1. Moment–curvature analysis

In order to accurately estimate the moment–curvature curves, the advanced section of analysis method was introduced in this study, where the assumption of plane section and negligible welding residual stress was made. Although the reduction in the interface fracture toughness under the moisture and temperature condition [30], the interface stress redistribution due to the long-term load [25], and the different failure paths under different chemical environment [31] were reported in the literature, the work in this paper is only focused on the short-term behavior and the slip effect is ignored. Thus, the perfect interface was introduced in the analysis. Similar assumptions were made in several literatures [28,33,11]. Because the local buckling only occurred in the fibers under compression, no hardening contribution was considered in the compressive branch. Therefore, Varma [48] has developed a stress–strain relationship to consider the local buckling of compression steel, in which the compression fibers were assumed to follow an elasto-plastic law. The idealized stress–strain curve in tension was given as follows:

$$\sigma = \begin{cases} E_s\varepsilon & 0 \leqslant \varepsilon \leqslant \varepsilon_y \\ f_y & \varepsilon_y < \varepsilon \leqslant \varepsilon_{sh} \\ f_u - (f_u - f_y)\left(\frac{\varepsilon_u - \varepsilon}{\varepsilon_u - \varepsilon_{sh}}\right)^k & \varepsilon_{sh} < \varepsilon \leqslant \varepsilon_u \end{cases} \tag{5}$$

Considered the normal strength of steel used in this study, the power of the hardening rule, k, was taken as 3 [48].

The concrete tensile strength was ignored when the tensile stress exceeded the ultimate tensile strength. For concrete compression, the stress–strain relationship proposed by Tomii and Sakino [42,43] is shown in Fig. 8(a). The width to thickness ratio (B/t) was the main influencing parameter to take account into the confinement effect. Because the confinement effect would only occur after a certain amount of plastic strain accumulation, thus the Hognestad model was used for the ascending branch of concrete stress–strain relationship, which was widely used for unconfined concrete.

The stress–strain relationship of prestressed strand can be illustrated by the Ramberg–Osgood curve [38] as shown in Fig. 8(b). When the stress is less than 70% of ultimate strength (f_{pu}), the stress increased linearly with the strain. When the stress exceeds 0.7 f_{pu}, the stress–strain relationship has multiple curves. The stress–strain relationship of prestressed strand is given as follows:

$$\sigma_{ps} = \begin{cases} E_p\varepsilon_{ps} & (\sigma_{ps} \leqslant 0.7f_{pu}) \\ \dfrac{E'\varepsilon_{ps}}{\left[1+\left(\frac{E'\varepsilon_{ps}}{f_{pu}}\right)^m\right]^{1/m}} & (\sigma_{ps} > 0.7f_{pu}) \end{cases} \tag{6}$$

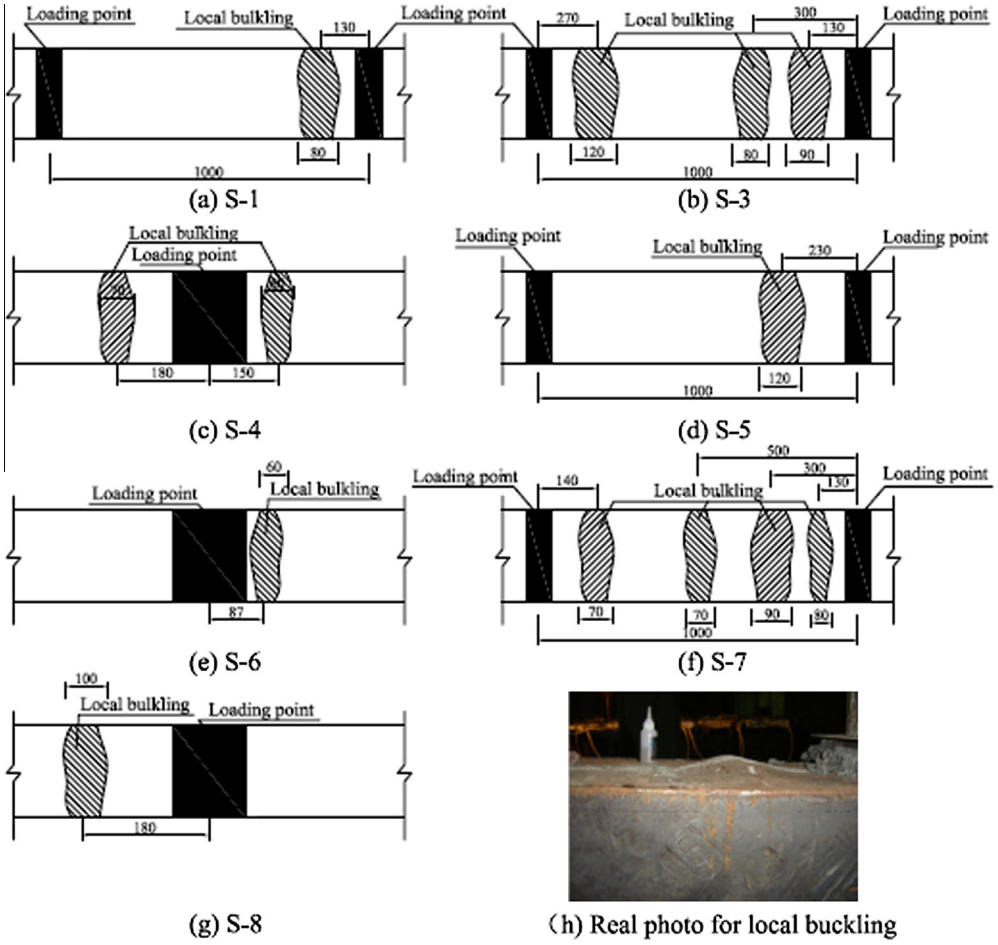

Fig. 7. Sketches of local buckling (unit: mm).

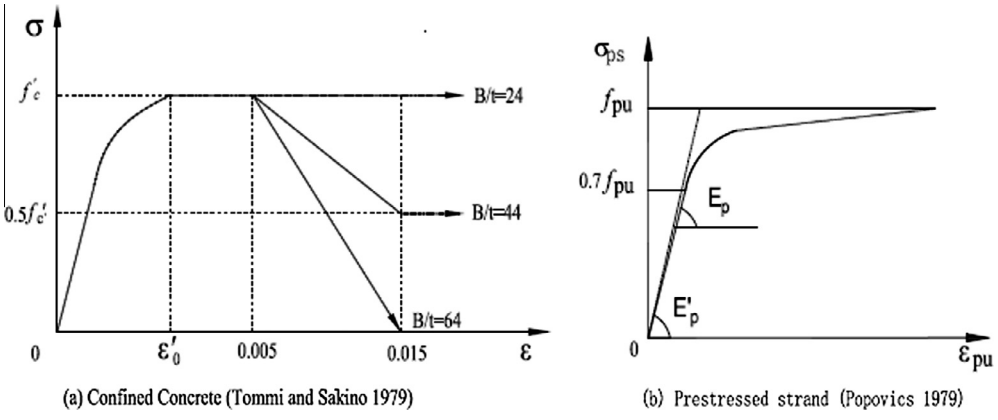

Fig. 8. Stress–stain relationships of concrete and prestressed strand.

Table 11
Analysis models.

Analysis model	Steel model		Concrete	Prestressed strand
	Tension	Compression		
Unconfined	Strain hardening (Varma)	Elastio-Plastic	Unconfined (Hongestad)	Ramberg–Osgood
Confined	Strain hardening (Varma)	Elastio-Plastic	Confined (Tomii and Sakino)	Ramberg–Osgood

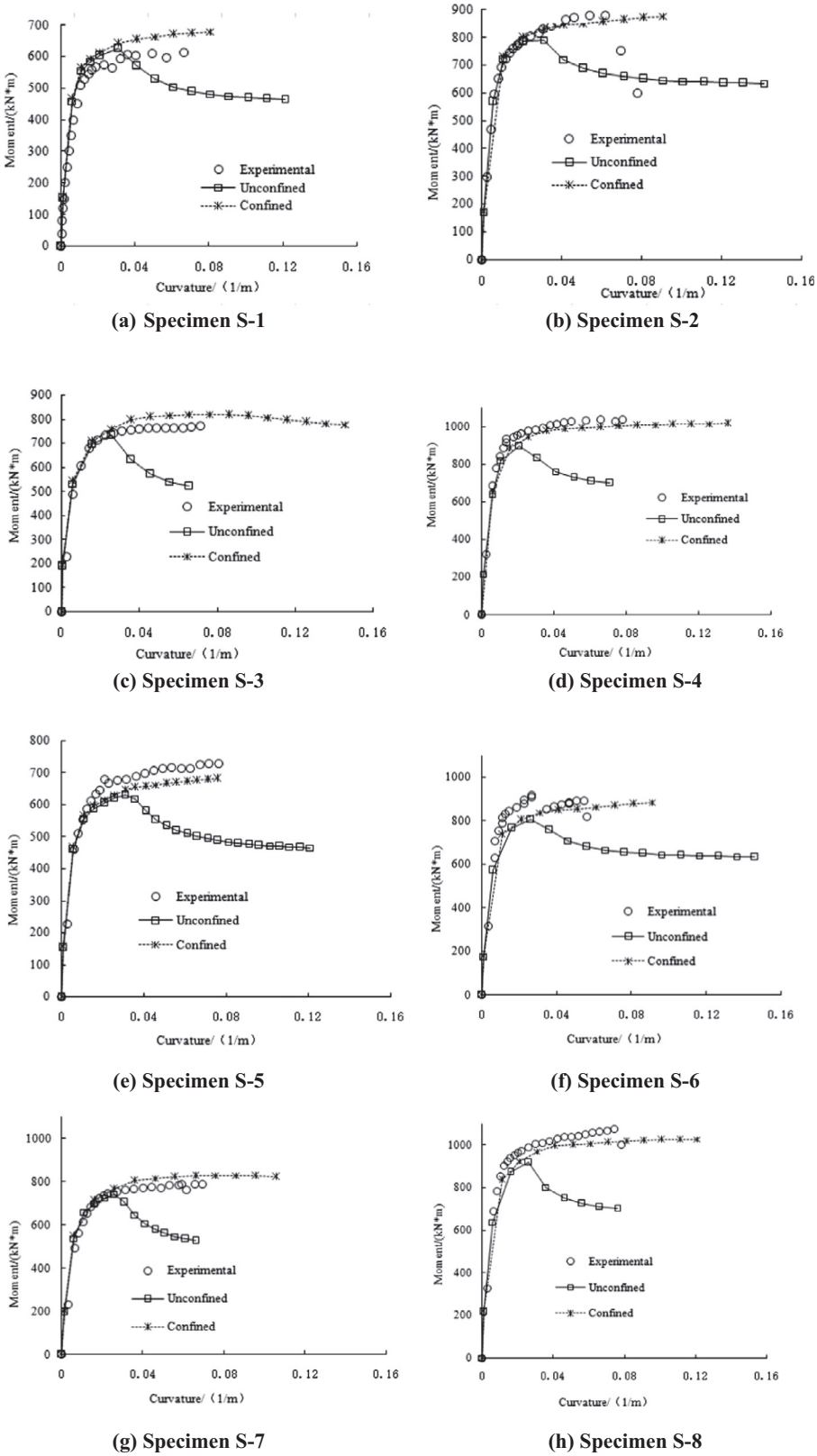

Fig. 9. Moment–curvature curves.

where σ_{ps}, ε_{ps} = stress and strain of prestressed strand, respectively; E_p = the Young's modulus of prestressed strand; E' = the slop at the original point of Ramberg–Osgood curve. In this study, E' was taken as 214.0 GPa; m = the coefficient for Ramberg–Osgood curve shape, and "m" was taken as 4.0.

To check the confinement effect of a large-scale section prestressed CFST beam, two different analysis models (i.e. unconfined and confined models) were summarized in Table 11. The moment–curvature curves are illustrated in Fig. 9(a)–(h) for the specimen S-1 ~ S-8. At the earlier loading stage, results of both unconfined

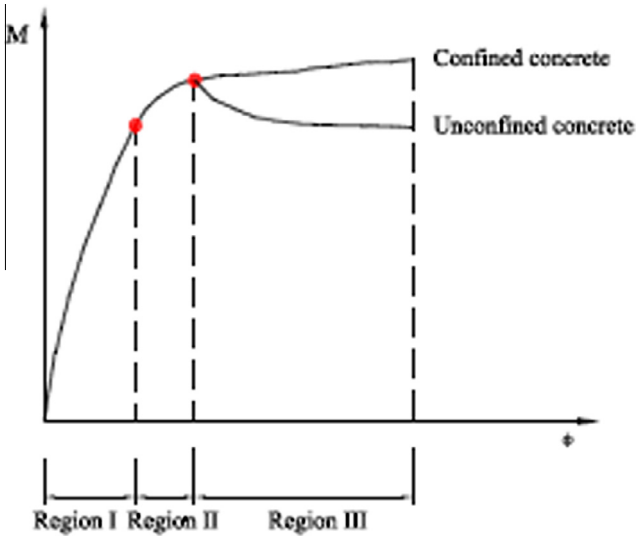

Fig. 10. Comparison of moment–curvature curves.

and confined models were in accordance with the testing ones. This can be explained by the fact that the confinement effect only occurs when the plastic strain accumulates to a certain level. At the later loading stage, it was found that the confined concrete model showed a closer agreement with the experimental result. Compared with the confined model and testing results, it was also found that the moment kept almost a constant value after yielding and did not drop rapidly until the deformation was large. In other words, it was proved that the prestressed CFST has an excellent ductility. This can be ascribed to the fact that the steel tube and prestressed strand contributed to the majority of moment capacity and the confined concrete increased the ductility. To explain the increased ductility characteristics of prestressed CFST beam, the moment–curvature relationship is shown in Fig. 10. From Fig. 10, the moment–curvature curve can be divided into three regions. Region I is the approximate elastic stage. In this region, both concrete and steel exhibits elastic behaviors until the steel begins to yield. Region II is the yielding stage of the steel and prestressed strand. Region III is the hardening stage. In this region, the concrete begins to exhibit the confinement effect while the steel gradually hardens. It is in this region where a significant confinement effect is observed, because it only occurs when the concrete plastic strain accumulates to a certain level.

4.2. Enhancement of prestressed strand

In order to investigate the enhancement of prestressed strand for CFST member under bending, an analytical model was developed by removing the prestressed strands. According to the results by Han [22], the normal concrete stress–strain constitutive relationship should be used to replace the confined law. The results of randomly selected S-2 and S-5 are shown in Fig. 11. It shows that the moment-deflection curves of normal CFST and prestressed CFST are consistent before the load reached the peak value. After the loading exceeded the peak moment, the curve of prestressed CFST kept the steady growth while the curve of normal CFST dropped rapidly. The reason for this phenomenon is that the prestressed strands are effective not only to prevent the crack but also to confine core concrete under bending. In addition, the ultimate moment of prestressed CFST has increased compared with the normal CFST. The enclosed area of prestressed CFST in moment-deflection curve is also much larger than that of normal CFST, which indicates that a prestressed CFST member has a better ductility than normal CFST member. In other words, the prestressed strands provide a significant enhancement to the CFST member.

4.3. Ultimate moment prediction

Flexural strength of a CFST member can be obtained from the current specifications. However, these specifications cannot be directly applied to a prestressed CFST beam. The plastic stress distribution is clearly preferred for the evaluation of the CFST bending strength [39,55]. At ultimate strength state, the ultimate tensile strength (f_u) rather than yield strength of steel was proposed in this paper for two reasons: (1) the ultimate tensile strength can take into account the large deformation and strain hardening [55]; (2) the ultimate tensile strength model can include the confinement and the final plastic failure mode [55,52]. A reduction factor (S) for the steel compressive stress was introduced to consider the incomplete plastic in the compression zone [4]. The effect of perfobond rib shear connector was not considered in the moment capacity prediction [29]. AISC-LRFD (2010) ignores the contribution of the filling concrete when predicting the ultimate moment, i.e. the ultimate moment is determined from a plastic stress distribution on the steel section alone. The stress distribution of the filled concrete according to AIJ [4] is shown in Fig. 12. The filled concrete in the tension zone of the section is assumed to be cracked and is therefore neglected. According to AIJ [4], the coefficient of k_1, k_2, γ_u and S are given as following:

$$k_1 = 0.831 - 0.076(\gamma_u f_c'/41.2) \geqslant 0.65 \quad (7)$$

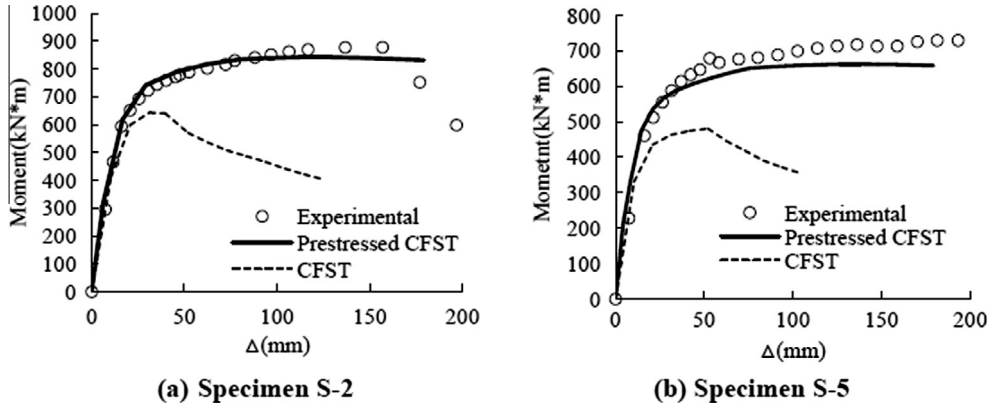

Fig. 11. Prestressed strand enhancement results.

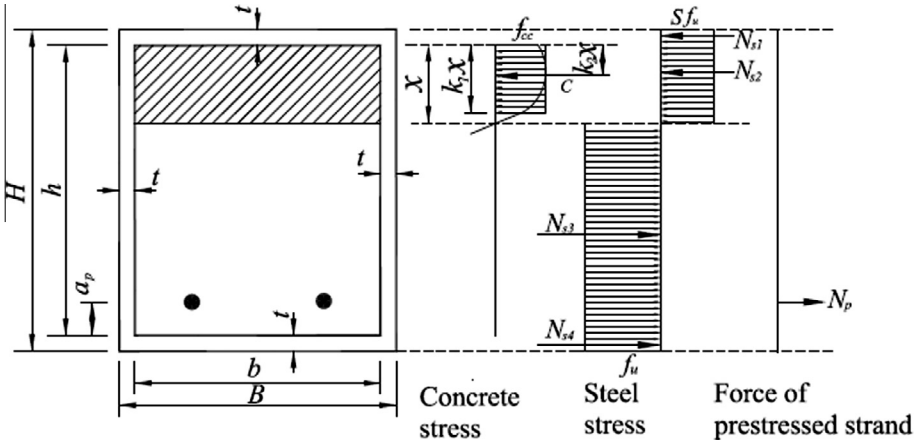

Fig. 12. Basic assumptions for plastic stress distribution method.

Table 12
Ultimate moment capacity comparisons.

Specimens	M_{u_AISC} (kN·m)	M_{u_AIJ} (kN·m)	M_u (kN·m)	M_{u_AISC}/M_u	M_{u_AIJ}/M_u
S-1	405.19	617.63	611.40	0.66	1.01
S-2	557.06	849.34	878.63	0.63	0.97
S-3	466.91	708.01	770.40	0.61	0.92
S-4	618.77	946.46	1037.88	0.60	0.91
S-5	405.19	624.88	729.10	0.56	0.86
S-6	557.06	860.69	893.63	0.62	0.96
S-7	466.91	721.47	790.10	0.59	0.91
S-8	618.77	953.23	1072.50	0.58	0.89
Average				0.61	0.93

$$k_2 = 0.429 - 0.010(\gamma_u f_c'/41.2) \tag{8}$$

$$\frac{1}{S} = 0.698 + 0.073\left(\frac{B}{t}\right)^2 \times \frac{f_y}{E_s} \geqslant 1.00 \tag{9}$$

$$\gamma_u = 1.67(1.13b)^{-0.112} \tag{10}$$

$$f_{cc} = \gamma_u f_c' \tag{11}$$

where f_{cc} = the compression strength of the filled concrete; f_c' = the compression strength of normal concrete; t = the thickness of steel tube; b = the inner width of the steel tube.

The position of the neutral axis can be attained using equilibrium conditions of forces as following:

$$N_{s1} + N_{s2} + C = N_{s3} + N_{s4} + N_{sp} \tag{12}$$

where N_{s1} = the force of upper compressive flange zone for steel tube; N_{s2} = the force of compressive web zone for steel tube; N_{s3} = the force of tension web zone for steel tube; N_{s4} = the force of underside tension flange zone for steel tube; C = the force of compressive flange zone for filled concrete.

The ultimate moment, M_{u_p}, can be derived using equilibrium conditions of moment as following:

$$\begin{aligned} M_{u\_p} = M_c + M_{s1} + M_{s2} + M_{s3} + M_{s4} + M_{ps} &= k_1(1-k_2)f_{cc}bx^2 \\ &+ Sf_u bt\left(x + \frac{t}{2}\right) + Sf_u t(x+t)^2 + Sf_u t(h-x+t)^2 \\ &+ f_u bt\left(h - x + \frac{t}{2}\right) + A_p f_p(h - x - t - a_p) \end{aligned} \tag{13}$$

where x = the height of compression concrete; b = the inner height of the steel tube; f_p = the ultimate strength of prestressed strand; a_p = the distance from the center of prestressed strands to the outside edge of steel tube.

The comparisons between the calculation and testing results are shown in Table 12, in which the ultimate moment calculated by the plastic analysis method of AISC-LRFD (2010) is also presented. It shows that the predicted ultimate moment by AIJ [4] agrees with the testing result better than that of AISC-LRFD (2010).

5. Conclusions

Eight prestressed CFST beams with large-scale section (300 × 450 mm) were tested under flexure. Two concrete strengths (C50 and C60) and two different degrees of prestressing (0.26 and 0.40) were studied in the experimental program. An analysis model was proposed to analyze the moment–curvature curves. Plastic stress distribution method was introduced to predict the ultimate moment capacity. Experimental and analytical results show that the prestressed effects enormously enhance the performance of CFST beams. The following conclusions can be drawn:

(1) The prestressed strands delay the crack occurrence and enhance the confinement effect of the core concrete, which, in turn, improve the composite action under bending. The cracking moment of prestressed CFST members is about 400% larger than that of non-prestressed CFST members.
(2) The prestressed CFST members show an excellent performance in terms of their moment strength capacities. The width-to-thickness (B/t) ratio is found to have a considerable impact on the ultimate moment capacity.
(3) The flexural stiffness of prestressed CFST members is superior to that of non-prestressed CFST members because of the efficacious confinement effect. The equivalent stiffness calculated from AISC-LRFD, EC4 and AIJ is only about 56%, 75% and 50% of that obtained from the experiment, respectively.
(4) The prestressed CFST beam exhibits a much higher ductility than non-prestressed CFST beam. An enormous increase in the ductility is observed, which is similar in the behavior to that of a concrete-filled steel tube column. There exists an obvious descent branch in the moment–curvature curves of non-prestressed CFST when comparing with prestressed CFST.

(5) Local buckling in compression flange was observed in most specimens, and no local buckling occurred in the web. The loading pattern has an impact to the local buckling, Four-point loading causes more serious local buckling than Three-point loading. The separation between the steel and concrete around local buckling point was observed.
(6) The results considering the confinement effect are in better agreement with the tests than that of unconfined concrete, which proves that the confinement effect exists in the large-scale prestressed CFST member when it subjected to bending.
(7) The ultimate moment capacity is derived based on the plastic stress distribution method. The results show that the AIJ method is better than other methods to predict the ultimate strength of prestressed CFST members.

Acknowledgements

The support from the National Natural Science Foundation of China (Grant 51208431, 51308468), the Fundamental Research Funds for the Central Universities (Grant SWJTU12CX064, 2682014CX072) is gratefully acknowledged. Visits to Southwest Jiaotong University by the third writer were made possible by Department of Civil & Environmental Engineering, University of Tennessee, Knoxville, USA.

References

[1] American Institute of Steel Construction (AISC). Load and resistance factor design (LRFD) specification for structural steel buildings, Chicago; 2010.
[2] ASTM. Test methods for tension testing of metallic materials. E8/E8M, West Conshohocken, PA; 2013.
[3] ASTM. Standard test methods for compressive strength test of cylindrical concrete specimens. C39/39M, West Conshohocken, PA; 2014.
[4] Architectural Institute of Japan (AIJ). Structural calculations of steel reinforced concrete structures, Tokyo, Japan; 1987.
[5] Bridge RQ. Concrete filled steel tubular columns. Report no. R283. Sydney (Australia): School of Civil Engineering, University of Sydney; 1976.
[6] Cavell DG, Waldron P. A residual strength model for deteriorating post-tensioned concrete bridges. Comput Struct 2001;79:361–73.
[7] Chen LM, Zhuang YZ, Zhu HY, Lu SJ. Application and theory of prestressed concrete-filled steel structure subjected to bending moment. J Zhejiang Univ (Eng Sci) 2002;36(5):549–52.
[8] Chitawadagi MV, Narasimhan M. Strength deformation behaviour of circular concrete filled steel tubes subjected to pure bending. J Constr Steel Res 2009;65:1836–45.
[9] Choi YH. A modified AISC P-M interaction curve for square concrete filled tube beam-columns Ph.D dissertation. University of Illinois at Urbana-Champaign; 2004.
[10] Commission of European Communities (CEN). Design of composite steel and concrete structures—Part-1: General rules and rules for building (EC4), Brussels; 2004.
[11] Eichalakani M, Zhao XL. Concrete-filled steel circular tubes subjected to pure bending. J Constr Steel Res 2004;57:1141–68.
[12] Eichalakani M, Zhao XL. Concrete-filled steel circular tubes subjected to constant amplitude cyclic pure bending. Eng Struct 2004;26(14):2125–35.
[13] Eichalakani M, Zhao XL. Concrete-filled cold-formed circular steel tubes subjected to variable amplitude cyclic pure bending. Eng Struct 2008;30:287–99.
[14] Eichalakani M, Zhao XL, Grzebieta RH. Concrete-filled circular steel tubes subjected to pure bending. J Constr Steel Res 2001;57:1141–68.
[15] Fukumoto Y. Structural stability design, steel and composite structure. Oxford: Pergamon; 1997.
[16] Furlong RW. Strength of steel-encased concrete beam-columns. J Struct Div, ASCE 1967;93(ST5):113–24.
[17] Gardner NJ, Jacobson ER. Structural behaviour of concrete filled steel tubes. J ACI 1967;64(7):404–13.
[18] Gho WM, Liu DL. Flexural behaviour of high-strength rectangular concrete-filled steel hollow sections. J Constr Steel Res 2004;60:1681–96.
[19] Gourley BC, Tort C, Hajjar JF, Schiller PH. A synopsis of studies monotonic and cyclic behavior of concrete-filled steel tube beam-columns. Structural engineering report No. ST-01-4, University of Minnesota, MN; 2001.
[20] Gourley BC, Hajjar JF. Cyclic nonlinear analysis of three-dimensional concrete-filled steel tube beam-columns and composite frames. Structural engineering report NO. ST-94-3. University of Minnesota, MN; 1994.
[21] Hajjar J. Concrete-filled steel tube columns under earthquake loads. J Progr Struct, Eng Mater 2000;2(1):1–10.
[22] Han LH. Flexural behaviour of concrete-filled steel tubes. J Constr Steel Res 2004;60:313–37.
[23] Hancock GJ, Zhao XL. Research into the strength of cold-formed tubular sections. J Constr Steel Res 1992;23:55–72.
[24] Han LH, Lu H, Yao GH, Liao FY. Further study on the flexural behaviour of concrete-filled steel tubes. J Constr Steel Res 2006;62:554–65.
[25] Hmidan A, Kim YJ, Yazdani S. Effect of sustained load combined with cold temperature on flexure of damaged steel beams repaired with CFRP sheets. Eng Struct 2013;56:1957–66.
[26] Jiang AY, Chen J, Jin WL. Experimental investigation and design of thin-walled concrete-filled steel tubes subject to bending. Thin-walled Struct 2013;63:44–50.
[27] Key PW, Hasan SW, Hancock GJ. Column behaviour of cold-formed hollow sections. J Struct Eng, ASCE 1988;114(2):390–407.
[28] Kilpatrick AE, Rangan BV. Tests on high-strength composite concrete columns. Research report, No. 1/97. Australia: Curtin University of Technology; 1997.
[29] Kim HY, Jeong YJ. Ultimate strength of a steel-concrete composite bridge deck slab with profiled sheeting. Eng Struct 2010;32:534–46.
[30] Lau D, Büyüköztürk O. Fracture characterization of concrete/epoxy interface affected by moisture. Mech Mater 2010;42(12):1031–42.
[31] Lee H-Y, Qu J. Microstructure, adhesion strength and failure path at a polymer/roughened metal interface. J Adhes Sci Technol 2003;17(2):195–215.
[32] Lu FW, Li SP, Li DW, Sun GJ. Flexural behavior of concrete filled non-uni-thickness walled rectangular. J Constr Steel Res 2007;63:1051–7.
[33] Lu YQ, Kennedy DJL. The flexural behavior of concrete-filled hollow structural sections. Can J Civ Eng 1994;21(1):111–30.
[34] Naaman AE. Partially prestressed concrete: review and recommendations. J Prestr Concr Inst 1985;30(6):30–71.
[35] Nakamura SI, Momiyama Y, Hosaka T, Homma K. New technologies of steel/concrete composite bridges. J Constr Steel Res 2002;58(1):99–130.
[36] Park R, Paulay T. Reinforced concrete structure. Canada: John Wiley & Sons; 1975.
[37] Prion HGL, Boehme J. Beam-column behaviour of steel tubes filled with high strength concrete. Can J Civ Eng 1994;21:207–18.
[38] Popovics S. Review stress–strain relationships for concrete. J Am Concr Inst 1970;67(3):243–8.
[39] Roeder CW, Lehman DE, Bishop E. Strength and stiffness of circular concrete-filled tubes. J Struct Eng, ASCE 2010;136(12):1545–53.
[40] Shakir-Khalil H, Zegiche Z. Experimental behavior of concrete-filled rectangular hollow section columns. Struct Eng 1989;67(19):345–53.
[41] Thody R. Experimental investigation of the flexural properties of high-strength concrete-filled steel tubes MSc thesis. Seattle, WA, USA: University of Washington; 2006.
[42] Tomii M, Sakino K. Experimental studies on the ultimate moment of concrete filled square steel tubular beam-columns. Transact Arch Inst Jpn 1979 (275):55–63.
[43] Tomii M, Sakino K. Elasto-plastic behavior of concrete filled square steel tubular beam-columns. Transact Arch Inst Jpn 1979;280:111–20.
[44] Tuan CY. Aurora arch bridge. Concr Int, April; 2004. p. 64–7.
[45] Tuan CY. Flexural behavior of nonposttensioned and posttensioned concrete-filled circular tubes. J Struct Eng, ASCE 2008;134(6):1057–60.
[46] Uy B. Strength of concrete filled steel box columns incorporating local buckling. J Struct Eng, ASCE 2000;126(3):341–52.
[47] Uy B. Strength of short concrete filled high strength steel box columns. J Constr Steel Res 2001;57(2):113–34.
[48] Varma AH. Seismic behavior, analysis, and design of high strength square concrete filled steel tube(CFT) columns Ph.D dissertation. Lehigh University; 2000.
[49] Virdi KS, Dowling PJ. Bond strength in concrete filled steel tubes. IABSE proceeding, P-33/80; 1980. p. 125–39.
[50] Webb J, Beyton JJ. Composite concrete filled steel tube columns. In: Proceedings of structural engineering conference. Adelaide: The Institution of Engineers Australia; 1990. p. 181–5.
[51] Wheeler A, Bridge R. The behaviour of circular concrete-filled thin-walled steel tubes in flexure. In: 5th International conference on composite construction in steel and concrete, Mpumalanga, South Africa, Jul 1–23. p. 412–3.
[52] Wright HD. Local stability of filled and encased steel sections. J Struct Eng, ASCE 1994;121(10):1382–8.
[53] Xu W, Hou XZ, Xu F, Zhang XF. Study on external prestressed concrete-filled steel tubular flexural member. Appl Mech Mater 2011;94–96:1066–9.
[54] Zhao XL, Hancock GJ. Tests to determine plate slenderness limits for cold-formed rectangular hollow sections of grade C450. Steel Constr, Austr 1991;25 (4):2–16.
[55] Zhao XL, Grzebieta R. Void-filled SHS beams subjected to large deformation cyclic bending. J Struct Eng, ASCE 1999;125(9):1020–7.